ResearchGate

See discussions, stats, and author profiles for this publication at: https://www.researchgate.net/publication/234123090

Alzheimer's Disease and Amnestic Mild Cognitive Impairment Weaken Connections Within the Default-Mode Network: A Multi-Modal Imaging Study

Article *in* Journal of Alzheimer's disease: JAD · January 2013

DOI: 10.3233/JAD-121879 · Source: PubMed

CITATIONS
92

READS
1,156

5 authors, including:

David C. Zhu
Albert Einstein College of Medicine
158 PUBLICATIONS **4,670** CITATIONS
SEE PROFILE

Shantanu Majumdar
Vanderbilt University
11 PUBLICATIONS **140** CITATIONS
SEE PROFILE

Igor O Korolev
Michigan State University
12 PUBLICATIONS **764** CITATIONS
SEE PROFILE

Andrea Bozoki
Michigan State University
45 PUBLICATIONS **2,329** CITATIONS
SEE PROFILE

All content following this page was uploaded by Andrea Bozoki on 25 February 2015.

The user has requested enhancement of the downloaded file.

Journal of Alzheimer's Disease 34 (2013) 969–984
DOI 10.3233/JAD-121879
IOS Press

Alzheimer's Disease and Amnestic Mild Cognitive Impairment Weaken Connections Within the Default-Mode Network: A Multi-Modal Imaging Study

David C. Zhu[a,b,c,*], Shantanu Majumdar[a,c], Igor O. Korolev[a,c,d], Kevin L. Berger[a,c] and Andrea C. Bozoki[a,c,d]
[a]*Department of Radiology, Michigan State University, East Lansing, MI, USA*
[b]*Department of Psychology, Michigan State University, East Lansing, MI, USA*
[c]*Cognitive Imaging Research Center, Michigan State University, East Lansing, MI, USA*
[d]*Department of Neurology, Michigan State University, East Lansing, MI, USA*

Accepted 18 December 2012

Abstract. We applied a multi-modal imaging approach to examine structural and functional alterations in the default-mode network (DMN) that are associated with Alzheimer's disease (AD) and amnestic mild cognitive impairment (aMCI), a transitional phase between healthy cognitive aging and dementia. Subjects included 10 patients with probable AD, 11 patients with aMCI, and 12 age- and education-matched normal controls (NC). Whole-brain resting-state functional, diffusion-weighted, and volumetric magnetic resonance imaging (MRI) data as well as ^{18}F-fluorodeoxyglucose-based positron emission tomography (FDG-PET) data were acquired. We carried out resting-state functional MRI-based functional connectivity and diffusion MRI-based structural connectivity analyses using isthmus of the cingulate cortex (ICC) and the subjacent white matter as the seeds. Whole-brain group and region of interest-based analyses demonstrated that AD weakens the structural and functional connections between ICC and other regions within the DMN, consistent with regional reduction of metabolic activity and atrophy within the DMN. A progressive weakening trend of these connections was also observed from NC to aMCI and then AD, although significant differences between aMCI and the other two groups were not found. Overall, based on both FDG-PET and MRI results, the DMN appears to serve as a window to understanding structural and functional brain changes associated with AD and aMCI.

Keywords: Alzheimer's disease, default-mode network, diffusion MRI, FDG-PET, mild cognitive impairment, multi-modal imaging, resting-state fMRI

INTRODUCTION

Alzheimer's disease (AD) is a progressive, neurodegenerative brain disorder and the most common cause of dementia among older adults. Patients with AD exhibit a gradual decline in cognitive function, including memory loss, impaired decision-making capacity, and disorientation, as well as changes in personality and mood. These cognitive and behavioral changes are accompanied by histological changes including neuronal degeneration and abnormal protein deposition in the cerebral cortex [1]. Mild cognitive impairment (MCI) is a clinical syndrome considered to represent a transitional phase between healthy cognitive aging and dementia. In contrast to dementia, cognitive deficits observed with MCI are milder and typically do not interfere with an individual's ability to perform

*Correspondence to: David C. Zhu, Ph.D., 293 Farm Lane, Room 358, Michigan State University, East Lansing, MI 48824, USA. Tel.: +1 517 353 9432; Fax: +1 517 432 2849; E-mail: zhuda@msu.edu.

ISSN 1387-2877/13/$27.50 © 2013 – IOS Press and the authors. All rights reserved

activities of daily living. Importantly, patients with MCI have a significantly increased risk of developing dementia, with a 10–15% annual rate of progression [2]. The amnestic subtype of MCI (aMCI) is characterized by memory impairment and the greatest risk of progression to AD-type dementia. AD is characterized by well-established patterns of both generalized cortical and accentuated medial temporal lobe (MTL) atrophy on structural magnetic resonance imaging (MRI) [3] and reduced glucose metabolism in the temporoparietal and posterior cingulate cortices on ^{18}F-fluorodeoxyglucose-based positron emission tomography (FDG-PET) [4, 5]. Structural MRI and FDG-PET are currently used as adjuncts in clinical evaluation of AD and dementia.

Recent advances in MRI techniques have allowed researchers to investigate alterations in brain connectivity associated with AD and MCI from multiple perspectives, such as the change in functional connectivity measured by resting-state functional MRI (rs-fMRI) [6–9], and the change in structural connectivity assessed by diffusion-weighted MRI (DWI) [10–11]. One specific set of findings from rs-fMRI studies involves changes within the default-mode network (DMN) of the brain [12] associated with MCI [7, 13] and AD [14–17]. The DMN is characterized by "deactivation" on fMRI during cognitively demanding tasks in normal subjects. As reviewed by Buckner et al. (2008), the DMN includes the posterior cingulate cortex (PCC), medial prefrontal cortex (MePFC), inferior parietal lobule, lateral temporal cortex, and regions of the MTL, including the hippocampal formation, entorhinal cortex, and parahippocampal gyrus (PHG). These regions appear to be active in synchrony when the brain is "at rest" (when individuals are asked to do nothing while lying in the MRI scanner). Of note, the cingulum bundle interconnects multiple components of the DMN, including the MePFC, PCC, and MTL [18]. The PCC, or more generally the posterior cingulate cortex/retrosplenial cortex (PCC/RSC) [19], is not only part of the DMN but also shows prominent hypometabolism as one of the earliest findings on FDG-PET scans of AD and many MCI patients [4, 5, 20, 21]. The MTL processes information from prior experiences in the form of memories, the MePFC facilitates the flexible use of this information during the construction of self-relevant mental simulations, and the outputs of these two regions converge on the PCC/RSC for information integration [22]. Consequently, the structural and/or functional damage of these brain regions can lead to cognitive impairment, notably episodic memory loss.

Most studies have focused on the application of a single imaging modality to investigate MCI- and AD-related alterations in the DMN. In this study, we applied a multi-modal imaging approach to provide an integrated structural-functional understanding of DMN connectivity in patients with probable AD, patients with aMCI, and normal control (NC) subjects. First, we analyzed the FDG-PET data to establish a pattern of AD- and aMCI-related cerebral hypometabolism in our subject cohort and to confirm the seed placement at the PCC/RSC for subsequent use in the connectivity analyses. Second, we analyzed the rs-fMRI data to test the hypothesis that AD and aMCI weaken the functional connection between PCC/RSC and other parts of the DMN. Third, we conducted DWI-based fiber tractography to test the hypothesis that AD and aMCI weaken the structural connection between PCC/RSC and other parts of the DMN, especially with MePFC. Fourth, we examined whether the weakened functional connectivity within the DMN is associated with neuronal damage to the corresponding DMN regions, as reflected by the metabolic activity on FDG-PET and cerebral atrophy on volumetric MRI.

MATERIALS AND METHODS

Subjects

Eleven patients with mild-to-moderate probable AD, 11 aMCI patients, and 12 age- and education-matched healthy NC subjects were recruited to participate in this study. The study was approved by the Michigan State University Institutional Review Board. All subjects or their legal representatives provided written informed consent. All subjects were carefully screened to exclude those with a history of stroke, brain tumors, aneurysms, brain surgery, serious head injury, or other significant neurological disease, as well as those with uncontrolled diabetes, hypertension, and hypothyroidism. All subjects were also screened for MR-incompatible metallic implants. The Saint Louis University Mental Status examination (SLUMS) [23], Logical Memory 30-minute delayed recall (LM-dr) test, and the Geriatric Depression Scale (GDS) [24] were performed on each subject. For additional subject information, MMSE (Mini-Mental State Examination) [25] was also performed on AD and aMCI subjects. NC subjects were community-dwelling older adults recruited from the Greater Lansing area in Michigan. Specific inclusion criteria for NC subjects included minimum cutoff scores of 25 (out of 30) on the SLUMS

Table 1
Subject characteristics

	NC ($n=12$)	aMCI ($n=11$)	AD ($n=10$)	p-value
Age [years]	73.8 (6.5)	77.1 (6.6)	72.9 (7.9)	0.36
Gender [female/male]	7/5	3/8	3/7	0.24
Education [years]	16.2 (3.9)	14.8 (2.5)	14.5 (3.3)	0.45
SLUMS	27.2 (1.2)	23.6 (3.1)	11.9 (6.6)	<0.001
GDS	0.7 (0.6)	2.4 (1.8)	2.3 (2.8)	0.12
LM - delayed recall	12.9 (2.9)	5.6 (4.3)	2.1 (4.2)	<0.001
MMSE^{+}		27.7 (1.6)	20.2 (4.4)	<0.001
	2 ε2/3	1 ε2/3		
	7 ε3/3	1 ε3/3	1 ε3/3	
APOE Genotype^{++}		4 ε3/4	5 ε3/4	
		1 ε4/4	1 ε4/4	

Values are shown as mean (standard deviation). $^{+}$MMSE was not collected in NC. One MCI subject did not have MMSE. $^{++}$APOE results are only available on some subjects. NC = Normal Control, aMCI = amnestic Mild Cognitive Impairment, AD = Alzheimer's Disease, SLUMS = Saint Louis University Mental Status examination, GDS = Geriatric Depression Scale, LM = Logical Memory test, MMSE = Mini-Mental State Examination.

and 8 (out of 25) on the LM-dr. Additionally, GDS scores indicated that our subjects were free of clinical depression with the possible exception of one AD patient (GDS score of 9 out of 15). The AD and aMCI patients were recruited through the Memory Disorders Clinic in the Department of Neurology at Michigan State University and were diagnosed using standard criteria by a practicing neurologist (NINCDS-ADRDA criteria for clinically probable AD and Petersen criteria for aMCI) [26, 27]. Data from one AD patient were discarded due to excessive motion artifacts. Cognitive evaluation was not obtained on one NC subject due to inadequate English language skills, but she and her family confirmed that she did not have any cognitive or neurological deficits. Normal brain anatomy was confirmed by a practicing neuroradiologist. One aMCI and two NC subjects did not undergo PET imaging. Most subjects provided a 3 ml blood sample for APOE genotyping. The final subject cohort characteristics are summarized in Table 1.

FDG-PET acquisition

After 10 mCi injection of FDG, subjects relaxed in a dim-light condition for 30 minutes to allow the metabolic uptake of FDG. Then 3D data of the whole brain were acquired on a GE Discovery STE scanner (GE Healthcare, Waukesha, WI) over 9 minutes in three 3-minute dynamic frames. CT attenuation correction was used.

MRI acquisition

The MRI experiment was conducted on a GE 3T Signa® HDx MR scanner (GE Healthcare, Waukesha, WI) with an 8-channel head coil. During each session, first and higher-order shimming procedures were carried out to improve magnetic field homogeneity. To study resting-state brain function, echo-planar images, starting from the most inferior regions of the brain, were acquired for 7 minutes with the following parameters: 38 contiguous 3-mm axial slices in an interleaved order, time of echo (TE) = 27.7 ms, time of repetition (TR) = 2500 ms, flip angle = 80°, field of view (FOV) = 22 cm, matrix size = 64×64, ramp sampling, and with the first four data points discarded. Each volume of slices was acquired 164 times while a subject was asked to relax and keep his/her eyes open in a dim-light condition, similar to that during metabolic uptake of FDG in PET scan. After the functional data acquisition, diffusion-weighted images were acquired with a dual spin-echo echo-planar imaging (EPI) sequence for 12 minutes and 6 seconds with the following parameters: 48 contiguous 2.4-mm axial slices in an interleaved order, FOV = 22 cm×22 cm, matrix size = 128×128, number of excitations (NEX) = 2, TE = 77.5 ms, TR = 13.7 s, 25 diffusion-weighted volumes (one per gradient direction) with $b = 1000$ s/mm^2, one volume with $b = 0$ and parallel imaging acceleration factor = 2. Finally, 180 T_1-weighted 1-mm^3 isotropic volumetric inversion recovery fast spoiled gradient-recalled images (10 minute scan time), with cerebrospinal fluid (CSF) suppressed, were obtained to cover the whole brain with the following parameters: TE = 3.8 ms, TR of acquisition = 8.6 ms, time of inversion (TI) = 831 ms, TR of inversion = 2332 ms, flip angle = 8°, FOV = 25.6 cm×25.6 cm, matrix size = 256×256, slice thickness = 1 mm, and receiver bandwidth = ±20.8 kHz.

Volumetric MRI Processing

One challenge in aging and AD brain imaging research is the high degree of anatomical variability due to brain atrophy, leading to difficulty in performing group-wise image analyses and tissue segmentation. FreeSurfer [28], an automated software for cortical surface reconstruction and anatomical segmentation of brain MRI scans, was found to have a robust performance in this regard. We processed all high-resolution T_1-weighted MR volumetric images through the default FreeSurfer processing stages to perform non-linear registration (warping) from the

original space to the MNI305 space (standard space), cortical and subcortical segmentations, and regional volume and cortical thickness measurements. We visually confirmed the accuracy of warping the T_1-weighted MR volumetric images to the standard space. For each warping step, a transformation matrix was created by FreeSurfer for each subject, which was used to warp the results of functional and structural connectivity maps to the standard space. All whole-brain group analyses were carried in the standard space. Anatomical regions segmented with FreeSurfer were applied to all region-of-interest (ROI) based connectivity, atrophy, and metabolic data analyses described later.

PET data processing

For each subject, simulated PET images were first created from the original T_1 volumetric images [29]. The original PET images were linearly registered to the simulated PET images (and thus to the T_1 volumetric images) using the "FLIRT" routine in the FSL software package [30]. The warped PET images were intensity-normalized by the mean signal of a 7 mm-radius sphere at the center of the pons [5]. ROI-based analyses were carried out on these normalized PET images. The whole-brain between-group analyses were done in MNI305 space after the normalized PET images were warped to the MNI305 standard space using the transformation matrix generated using FreeSurfer as discussed earlier.

Generation of seed regions for connectivity analyses

We selected relatively small-size, anatomically-defined regions based on the FreeSurfer [28] segmentation as seeds for connectivity analyses in this work, including right and left isthmi of the cingulate cortex (ICCs), and right and left hippocampi. Each of these regions is well-defined by FreeSurfer, with reasonable volumes for connectivity analyses (means of 2089/2381 mm^3 for the right/left ICCs and 3494/3400 mm^3 for the right/left hippocampi for the NC group). The ICCs defined in FreeSurfer overlaps with the boundaries of the PCC/RSC (L1, P50, S26), defined by Andrews-Hanna et al. (2007) for their connectivity analyses of the DMN. The right and left hippocampi are also part of the DMN [4, 22] and are known to be affected by AD. To obtain the corresponding structural connectivity, white matter (WM) regions immediately subjacent to the ICCs were used as seed regions for DWI-based fiber tracking. These WM regions were defined using FreeSurfer [28] to include WM tissue within 5 mm of the gray/white matter boundary. This approach allows for integrated understanding of the functional and structural connectivity from a common anatomical region (see Figs. 1a and 2a).

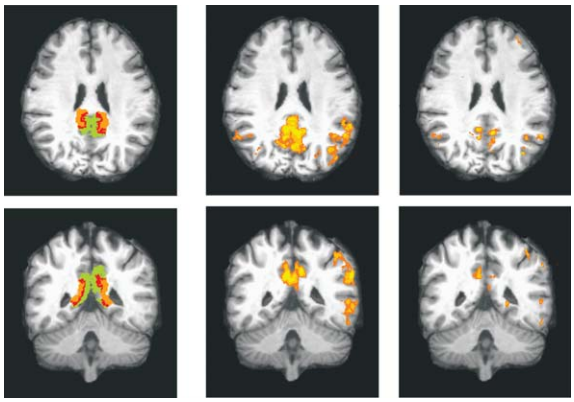

Fig. 1. (a) The right and left isthmus of cingulate cortex (ICC) seeds are shown (Green: gray matter, Orange: white matter, Red: gray-white matter border). Significant differences ($p \leq 0.049$) on the normalized PET signal were shown for (b) Normal > AD, (c) Normal > aMCI at the corresponding seed regions.

Demographic and cognitive data analyses

SPSS (version 19) was used to analyze subject characteristics. Between-group differences were tested using one-way ANOVA for all variables except gender, where a chi-square test was used instead. *Post-hoc* comparisons were made using the Tukey HSD test. The homogeneity of variances assumption was violated for SLUMS and GDS score variables, as indicated by Levene's test, so we applied the Brown-Forsythe and Games-Howell adjustments to the *F*-statistic and *post-hoc* tests, respectively. Statistical significance was set at $p \leq 0.05$.

Resting-state fMRI individual-subject data processing

Resting-state fMRI correlation analysis was conducted using AFNI software [31] in the original space. For each subject, the acquisition timing difference was first corrected for different slice locations. With the last functional volume as the reference,

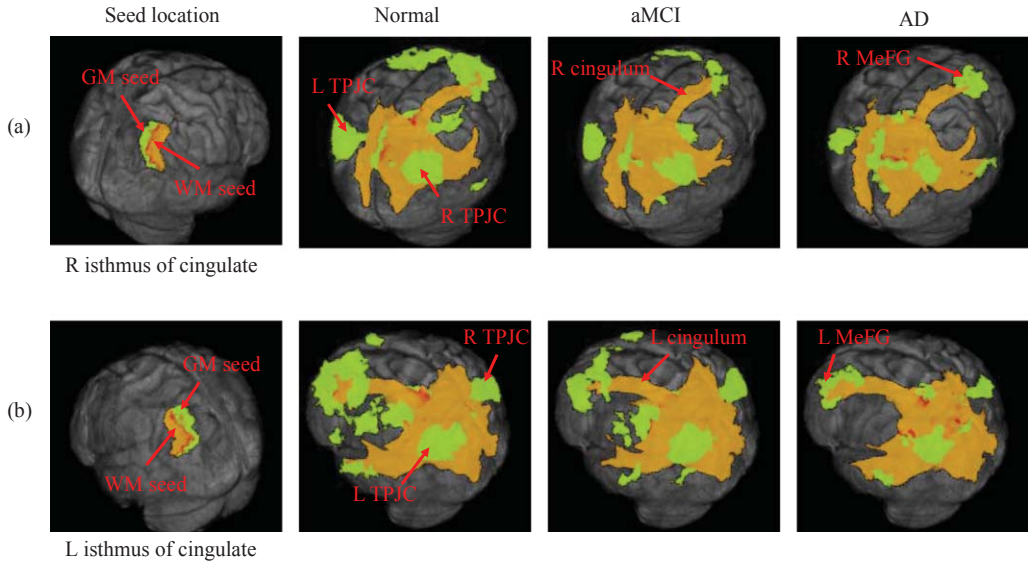

Fig. 2. The integrated visualization of the functional and structural connections for Normal, aMCI, and AD subjects (left to right) with the seed regions (GM and WM) of (a) right isthmus of cingulate cortex (ICC) and (b) left ICC. Thresholds: whole-brain corrected $p \leq 0.033$ for functional connectivity and mean connectivity distribution of > 1000 for structural connectivity. Green: functional connection only. Orange: structural connection only. Red: coexistence of both connections. GM: gray matter. WM: white matter. *R* = right. *L* = left. MeFG = medial frontal gyrus. TPJC = temporoparietal junction cortices.

rigid-body motion correction was done in three translational and three rotational directions. The amount of motion was estimated and then modeled in data analysis. For each subject, spatial blurring with a full width half maximum (FWHM) of 4 mm was used to reduce random noise and inter-subject anatomical variation during group analysis. At each voxel, motion-estimation parameters, baseline, linear and quadratic system-induced signal trends were removed from the time courses using the "3dDeconvolve" routine in AFNI [32]. Brain global, CSF, and WM mean signals were modeled as nuisance variables and removed from the time courses as well. In order to create the time course from pure CSF regions, the lateral and 3rd ventricles on the high-resolution T_1-weighted volumetric images were segmented using FreeSurfer software followed by 1 mm^3 erosion [28]. For the same reason, the WM was segmented from the T_1-weighted volumetric images using the "FAST" routine in the FSL software [30] followed by 4 mm × 4 mm × 4 mm cubical erosion. The cleaned time courses were then band-pass filtered in the range of 0.009 Hz – 0.08 Hz [33]. These filtered time courses were used for correlation-based connectivity analyses. The "3dfim+" routine in AFNI [31] was used to correlate the time course in every voxel of the brain against the space-averaged time course from a seed region.

Resting-state fMRI between-group statistical comparison

To prepare for group analysis, the correlation coefficients were converted to *Z* values through Fisher's Z-transformation to improve the normality of the distribution. After warping to the MNI305 standard space, the data were spatially blurred with FWHM of 2 mm to reduce potential noise generated by non-linear warping. In group analysis, *t* tests were performed on the *Z* values between each pair of our three subject groups (NC, aMCI, and AD).

DWI fiber tracking and between-group statistical comparison

Probabilistic fiber tracking was performed using routines from the FSL Diffusion Toolbox (FDT v2.0) [30, 34, 35]. After eddy-current distortion and motion correction, Bayesian Estimation of Diffusion Parameters Obtained using Sampling Techniques with crossing fibers modeled ($n = 2$) (BEDPOSTX) [34] was performed at each voxel. Then, probabilistic tractography with the "PROBTRACKX" routine was applied to calculate whole-brain connectivity distributions from each ICC seed region. The connectivity distribution maps were then warped to the MNI305 standard space.

The data were spatially blurred with FWHM of 2 mm to reduce the noise due to non-linear warping. Between-group t tests on each pair of our three groups were performed.

Correction for multiple comparisons for group analyses and further processing

Monte Carlo simulation was performed according to the matrix and voxel size of the imaging volume, and voxel intensity thresholding, masking, and spatial blurring applied. Cluster identification was used to estimate overall statistical significance with respect to the whole brain [36]. For the PET data, spatial blurring of 6 mm FWHM was estimated as the effective blurring due to the image acquisition procedure for our PET scanner [37] and was used in Monte Carlo simulation. Based on these estimations, the between-group t-test results on PET data were corrected for multiple comparisons based on the following criteria: A voxel was considered significant only if it was within a 661 mm^3 cluster in which the voxels were connected and all had a voxel-based $p \leq 5 \times 10^{-3}$. Based on the application of these criteria to the whole brain, the voxel-based $p \leq 5 \times 10^{-3}$ was corrected to be an equivalent whole-brain $p \leq 0.049$. Similarly, the between-group t-test results for functional connectivity with ICC were corrected for multiple comparisons based on the following criteria: A voxel was considered significant only if it was within a 425 mm^3 cluster in which the voxels were connected and all had a voxel-based $p \leq 5 \times 10^{-3}$. Based on the application of these criteria to the whole brain, the voxel-based $p \leq 5 \times 10^{-3}$ was corrected to be an equivalent whole-brain $p \leq 0.033$. With the same statistical criteria, the DMN for the NC group was defined based on the positive functional connectivity to ICC versus random chance. The corrected between-group t-test results were further restricted to the DMN as defined using the NC group. For DWI-based structural connectivity, the between-group t-test results were similarly corrected for multiple comparisons based on the following criteria: A voxel was considered significant only if it was within a 30.8 mm^3 cluster in which the voxels were connected and all had a voxel-based $p \leq 5 \times 10^{-3}$. Based on the application of these criteria to the whole brain, a voxel-based $p \leq 5 \times 10^{-3}$ was corrected to an equivalent whole-brain $p \leq 0.028$. With the same statistical criteria, the DMN-related structural connections for the NC group were defined based on the connectivity distribution versus random chance. As with the functional connectivity analysis, the corrected between-group t-test results were restricted to the DMN-related structural connections defined using the NC group.

Integrated visualization of functional and structural connectivity of the ICC

The integration of functional and structural connectivity maps was done with a bitmap coding technique as done in Zhu et al. [38], color-coded for visualization as follows:

1 = functional connection only (green),
2 = structural connection only (orange), and
3 = coexistence of both (red).

The above integration was done at the group level after appropriate thresholding. Functionally connected regions were identified based on statistical criteria discussed earlier (whole-brain corrected $p \leq 0.033$). Structurally connected regions were defined based on a mean connectivity distribution threshold of >1000.

Relationships among functional connectivity, metabolic activity, and atrophy measures

To understand whether the functional connectivity decline is driven by neuronal damage, we correlated functional connectivity scores (Z-transformed correlation coefficients) for each pair of ROIs found to be affected in AD/aMCI patients with the normalized PET signal, volume, and cortical thickness measures for each of these two ROIs. The correlation between the normalized PET signal and volume and cortical thickness measures for each ROI was also performed. The significance level for all correlations and t tests was set at $p \leq 0.05$.

Brain-behavior correlation analyses

Brain-behavior correlation analyses were performed to investigate whether DMN functional connectivity explained the change of cognitive function. For these analyses, we first extracted the cleaned and filtered time courses from bilateral ICCs and hippocampi for each subject as described earlier. Pearson correlation coefficients were calculated between each pair of the four time courses. These coefficients were then converted to Z values through Fisher's Z-transformation. Next, Pearson correlation coefficients were calculated between cognitive performance scores (SLUMS or LM-dr) and the Fisher's Z-transformed values of the respective functional correlations across all subjects,

and then NC and AD only. The significance was set at $p \leq 0.05$.

RESULTS

Demographic and cognitive data

Table 1 shows subject characteristics for NC, aMCI, and AD groups. The three subject groups did not differ statistically with regard to age, gender composition, or educational attainment. SLUMS scores differed among the groups [$F(2,13) = 36.0, p < 0.001$], with NC exhibiting greater scores than both aMCI ($p = 0.008$) and AD ($p < 0.001$) and aMCI exhibiting greater scores than AD ($p = 0.001$). GDS scores did not differ statistically among groups. Scores on the LM-dr test differed among groups [$F(2,29) = 21.9$, $p < 0.001$], with NC exhibiting greater scores than both aMCI ($p < 0.001$) and AD ($p < 0.001$); aMCI and AD groups did not differ in this regard.

FDG-PET metabolic activity

The whole-brain between-group *t* tests show a progressive reduction in metabolic activity on a continuum from NC to aMCI and then AD, notably in the posterior regions of the DMN. Specifically, a significant progressive decline was seen in right and left PCC/RSC, including subregions of PCC/ICC and precuneus. Significant NC > AD and NC > aMCI metabolic activity differences were also found in the right and left-temporoparietal junction cortices (TPJC) (including subregions of the angular gyrus (AG), inferior parietal lobule (IPL), superior temporal gyrus (STG) and supramarginal gyrus (SMG)) and left MTL (left hippocampus/PHG). The right and left ICC seeds used for correlation-based connectivity analyses overlapped with the significant NC > AD and NC > aMCI metabolic activity clusters in the PCC/RSC region, as expected (Fig. 1).

Integrated visualization of functional and structural connectivity of the ICC

Integrated visualization of functional and structural connections demonstrates a general progressive weakening from NC to aMCI and then AD of the long-range structural connection from right ICC to MePFC, based on the length of the fiber tracts (Fig. 2a). Based on the spatial extent of the functionally-connected regions at MePFC, the functional connection from right ICC to MePFC is also weakened in both aMCI and AD relative to NC, but the change from aMCI to AD is not obvious. This progressive weakening trend is also seen for the functional connection from right ICC to right and left TPJCs. With the left ICC as the seed, the long-range functional connections demonstrate a similar progressive weakening from NC to aMCI and then AD (Fig. 2b). This progressive trend is not obvious for the fiber tracts from the left ICC, but notably, the mean fiber tract in the NC group appears to reach further to MePFC than in both the aMCI and AD groups. The above qualitative patterns were further evaluated through the following statistical comparisons.

Connectivity from the right ICC

Based on the *t* test between NC and AD, the NC group had significantly stronger functional connection than the AD group to the following regions: right TPJC (including subregions of STG, MTG, SMG, AG, and IPL, with the center around AG), PCC/RSC (including left CG, adjacent to PCC, and right precuneus), and left TPJC (including MTG, AG and precuneus) (Fig. 3, Table 2). These clusters coincide with the DMN [22]. The PET signal is significantly reduced at these regions due to AD as well (NC > AD), as presented earlier in the between-group PET analyses (Fig. 3d). However, *t* tests between NC and aMCI and between aMCI and AD did not show significant differences within the DMN.

Between-group *t* tests showed significantly stronger structural connections for the NC group compared to both AD and aMCI groups along the right cingulum and its anterior extension to MePFC (total sizes of 776 mm^3 for NC > AD and 1467 mm^3 of NC > aMCI) (Fig. 4). The *t* test between aMCI and AD did not show a significant difference along the cingulum and its anterior extension to MePFC.

Connectivity from the left ICC

The NC group had significantly greater functional connection than the AD group in the following regions: right hippocampus, PCC/RSC (including right PCC and left PCC/precuneus), and left SFG (Fig. 5, Table 3). The PET signal is significantly reduced at these PCC/RSC regions due to AD as well (NC > AD), as presented earlier in between-group PET analyses (Fig. 1b). The right hippocampus and the left SFG contained marginally significantly reduced PET signal due to AD (NC > AD with $p < 0.01$ before whole-brain correction based on PET analysis results presented earlier). The *t* tests between NC and aMCI

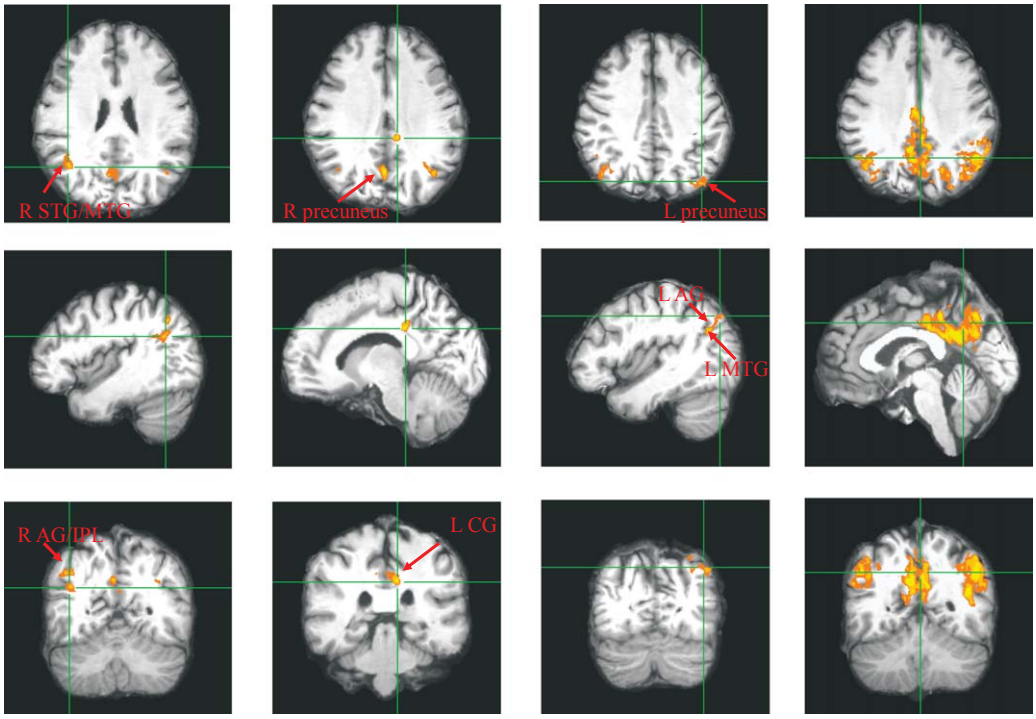

(a) RTPJC (b) PCC/RSC (c) L TPJC (d) PET: NC > AD

Fig. 3. With the seed regions at the right isthmus of cingulate cortex, the normal control group had significantly stronger functional connection than the AD group at the following regions (yellow and orange): (a) right TPJC (temporoparietal junction cortex), (b) PCC/RSC and (c) left TPJC. (d) Regions with significant NC > AD PET signal are shown for comparison. R = Right. L = Left. AG = angular gyrus. IPL = inferior parietal lobule. MTG = middle temporal gyrus. The green cross hairs indicate the location of the corresponding axial, sagittal and coronal views.

Table 2
Functional connectivity from the left isthmus of cingulate cortex: normal control versus AD

Cluster region	Size (mm^3)	Centroid coordinate	Mean correlation r	
			Normal	AD
Normal >AD				
PCC/RSC region				
Right precuneus	858	(R4, P65, S29)	0.654	0.429
Left CG	651	(L4, P35, S35)	0.51	0.275
Left TPJC region				
Left precuneus/AG/MTG	728	(L39, P70, S36)	0.418	0.179
Right TPJC region				
R IPL/AG	579	(R46, P62, S40)	0.401	0.185
R STG/MTG/SMG/AG	495	(R43, P58, S26)	0.424	0.168

CG = cingulate gyrus, AG = angular gyrus, MTG = middle temporal gyrus, IPL = inferior parietal lobule, STG = superior temporal gyrus, SMG = supramarginal gyrus. Coordinate is in MNI 305 standard space. *R* = right, *L* = left, *A* = anterior, *P* = posterior, *S* = superior, *I* = inferior.

and between aMCI and AD did not reach significant functional connectivity differences within the DMN. The between-group *t* tests did not reach significant differences in structural connectivity along the cingulum or its anterior extension either.

ROI-based PET-functional connectivity correlation

Significant correlations were found between the normalized PET signal (measurement of metabolic

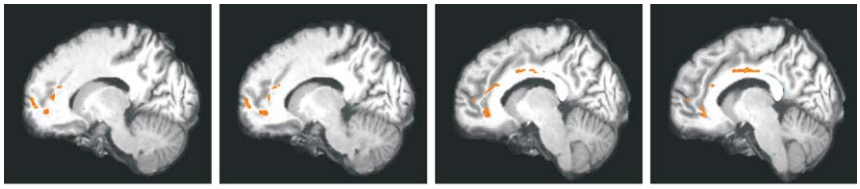

(a) NC > AD

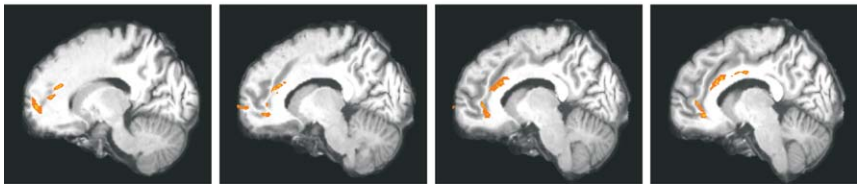

(b) NC > aMCI

Fig. 4. With the seed region in the associated white matter of the right isthmus of cingulate cortex, normal control (NC) subject show significantly stronger structural connections (yellow and orange) along the right cingulum and its anterior extension than both (a) AD and (b) aMCI subjects.

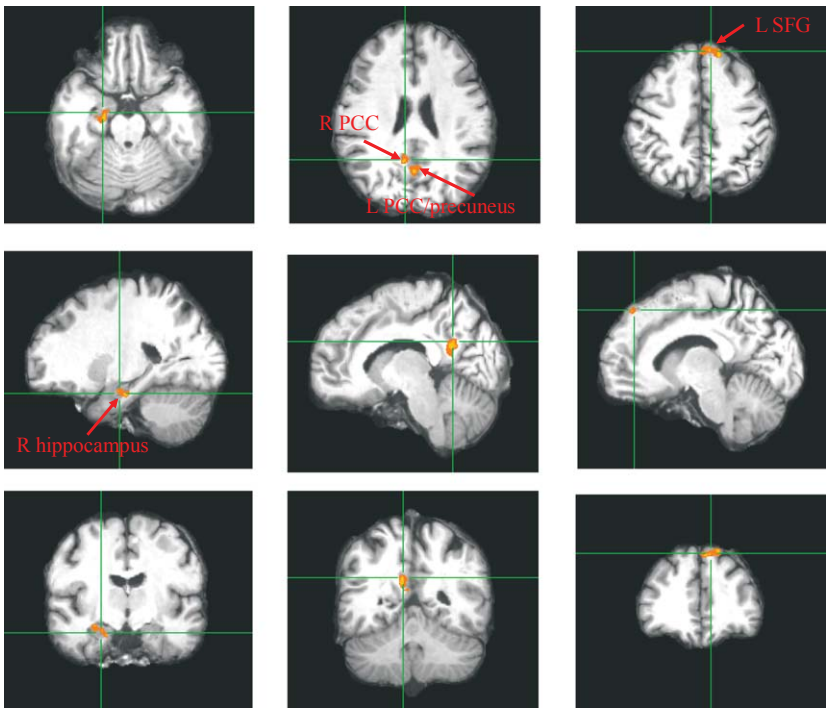

(a) (b) (c)

Fig. 5. With the seed regions at the left isthmus of cingulate cortex, the NC group had significantly higher functional connectivity than the AD group in the following regions (yellow and orange): (a) right hippocampus, (b) PCC/RSC, and (c) left superior frontal gyrus (SFG). R = Right. L = Left. The green cross hairs indicate the location of the corresponding axial, sagittal and coronal views.

activity) in all four ROIs (bilateral ICCs and bilateral hippocampi) and the functional connection between left ICC and right hippocampus (Table 4, Fig. 6). Significant correlations were also found between the normalized PET signal in both hippocampi and the functional connection between left ICC and left hippocampus (Table 4, Fig. 7). Between-group *t* tests on the normalized PET signal in bilateral ICCs, and bilat-

Table 3
Functional connectivity from the left isthmus of cingulate cortex: normal control versus AD

Cluster region	Size(mm^3)	Centroid coordinate	Mean correlation r	
			Normal	AD
Normal > AD				
PCC/RSC region				
Right and Left PCC/precuneus	837	(R3, P63, S29)	0.700	0.469
R PCC	572	(R10, P52, S21)	0.685	0.435
Left SFG	620	(L8, A41, S49)	0.317	0.044
R hippocampus	574	(R25, P15, I23)	0.211	−0.040

PCC = posterior cingulate cortex, SFG = superior frontal gyrus. Coordinate is in MNI305 standard space. R = right, L = left, A = anterior, P = posterior, S = superior, I = inferior.

Table 4
Normalized PET signal and functional connectivity correlation

Regions of interest	PET correlation to functional connectivity		t tests on PET signal (p value)		
	L ICC-R hippocampus	L ICC-L hippocampus	Normal > AD	Normal > aMCI	aMCI > AD
R ICC	0.365 (0.047)	0.317 (0.088)	0.0008	0.0140	0.1057
L ICC	0.374 (0.042)	0.355 (0.054)	0.0002	0.0011	0.0431
R hippocampus	0.364 (0.048)	0.382 (0.037)	0.0204	0.0014	0.7691
L hippocampus	0.392 (0.032)	0.426 (0.019)	0.0119	0.0015	0.5428

Numbers are show in correlation coefficient r (p value) for 2nd and 3rd columns. Functional connectivity is in Z transformation of correlation coefficient. R = right, L = left, ICC = isthmus of cingulate cortex.

eral hippocampi all showed significant reduction in AD and aMCI relative to NC. Of these four regions, only the left ICC PET signal showed a significant reduction from aMCI to AD (Table 4).

ROI-based cortical atrophy-functional connectivity correlation

Significant correlations were found between left ICC cortical thickness and both the left ICC-right hippocampus functional connectivity ($r = 0.469$, $p = 0.006$) and the left ICC-left hippocampus functional connectivity ($r = 0.410$, $p = 0.018$) (Fig. 8). Because the right and left ICC thicknesses were significantly correlated to each other ($r = 0.833$, $p < 0.001$), significant correlations were also found between the right ICC thickness and both the left ICC-right hippocampus functional connectivity ($r = 0.450$, $p = 0.009$) and the left ICC-left hippocampus functional connectivity ($r = 0.454$, $p = 0.008$). No other correlations between functional connectivity and the cortical thickness and volume values at the corresponding ROIs were found significant. Between-group t tests showed significant difference at both the right and left ICC thicknesses as well, specifically, at the right ICC, p values = 0.00006, 0.024, 0.005 for NC versus AD, NC versus aMCI and aMCI versus AD, respectively; at the left ICC, p values = 0.001, 0.014, 0.044 for NC versus AD, NC versus aMCI and aMCI versus AD, respectively.

PET-cortical atrophy correlation

With all subjects included, significant correlations were found between normalized PET signal and cortical atrophy (volume and/or cortical thickness) at each of the four ROIs defined (Table 5).

Brain-behavior correlation

With all subjects included, significant correlation was found between SLUMS score and the left ICC-right hippocampus functional connectivity ($r = 0.459$, $p = 0.0082$), and between LM-dr score and the above functional connectivity ($r = 0.375$, $p = 0.0347$) (Fig. 9). Examining only the NC and AD subjects, a significant correlation was also found between the left ICC-right hippocampus functional connectivity and SLUMS score ($r = 0.509$, $p = 0.0186$), and LM-dr score ($r = 0.452$, $p = 0.0396$).

DISCUSSION

In this study, we applied a multi-modal imaging approach to enhance the understanding of structural and functional alternations due to AD. We recruited three well controlled groups of subjects (NC, aMCI, and AD) and integrated the functional and structural connectivity analyses using subject-specific seed regions located at the isthmus of the cingulate cortex

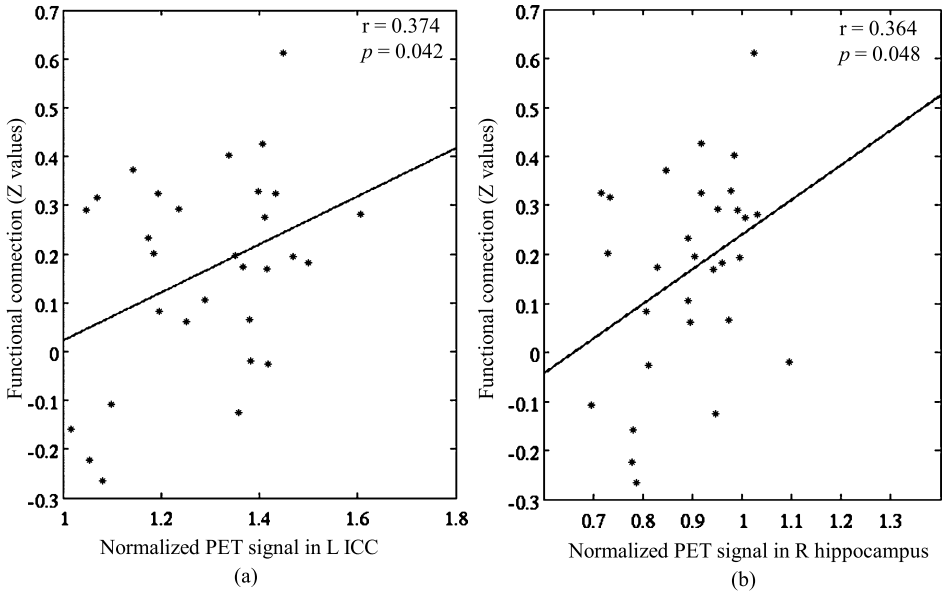

Fig. 6. With all subjects included, the significant correlations were shown between the left ICC-right hippocampus functional connection (the Fisher's Z-transformed values of the correlations) and the normalized PET signals in (a) left ICC and (b) right hippocampus. R = right, L = left and ICC = isthmus of cingulate cortex.

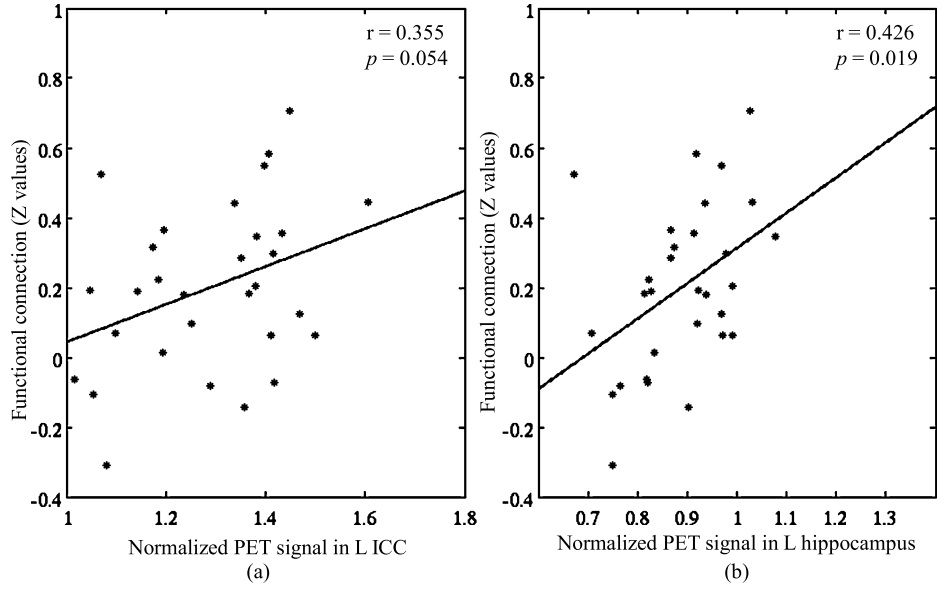

Fig. 7. With all subjects included, the significant correlations were shown between the left ICC-left hippocampus functional connection (the Fisher's Z-transformed values of the correlations) and the normalized PET signals in (a) left ICC and (b) left hippocampus. L = left and ICC = isthmus of cingulate cortex.

(ICC) and the subjacent white matter. To minimize the issue of anatomical variability due to brain atrophy in group-wise image analyses, we performed a non-linear warping technique to transform functional and structural connectivity maps as well as PET images to MNI305 standard space for group analyses. Our ROI-based cross-modal correlation analyses provided further understanding of the weakened connections due to AD. Overall, our hypotheses were supported by the results.

The NC, aMCI, and AD groups were well-matched for age, gender composition, and educational attain-

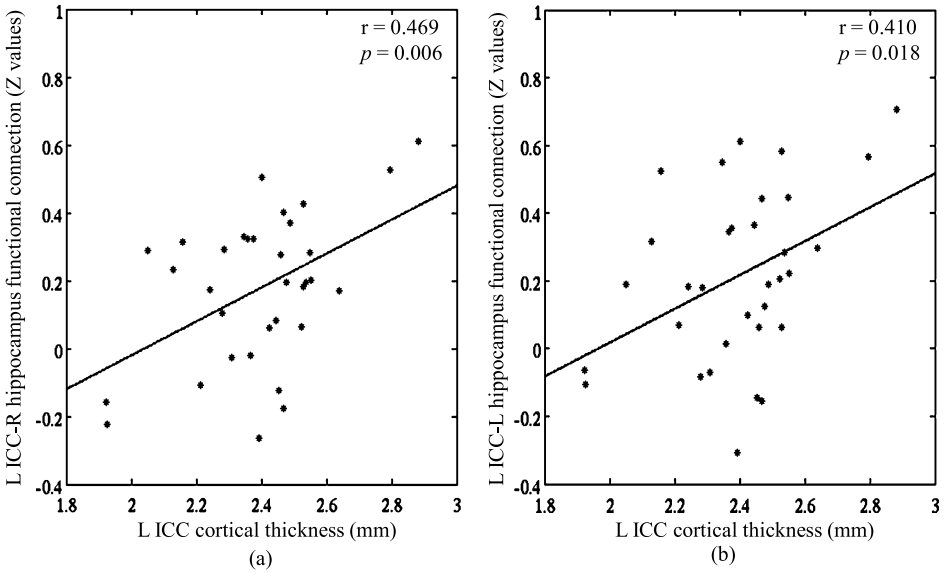

Fig. 8. With all subjects included, the significant correlations were shown between the left ICC cortical thickness and the functional connections (the Fisher's Z-transformed values of the correlations) between (a) the left ICC and right hippocampus, and (b) the left ICC and left hippocampus. R = right, L = left and ICC = isthmus of cingulate cortex.

Table 5
Normalized PET signal correlations with cortical atrophy

Region of interest	PET signal correlation with	
	Cortical volume	Cortical thickness
Right isthmus of cingulate cortex	0.383 (0.037)	0.603 (<0.001)
Left isthmus of cingulate cortex	0.385 (0.036)	0.677 (<0.001)
Right hippocampus	0.853 (<0.001)	N/A
Left hippocampus	0.788 (<0.001)	N/A

Numbers are shown in correlation coefficient *r* (*p* value).

ment. As expected, performance on the SLUMS (a global measure of cognitive function) declined sequentially from NC to aMCI and then AD. NC subjects also had significantly better episodic memory performance, as assessed by the LM-dr test, than both aMCI and AD subjects. Episodic memory performance is a characteristic deficit manifested by aMCI subjects, whose performance was statistically indistinguishable from AD subjects in these small groups with large test-score variability.

The between-group comparison of metabolic activity demonstrated that the posterior part of the DMN, notably the right and left PCC/RSC, the right and left TPJCs and the left MTL, were affected the most by aMCI and AD. This result is consistent with previous studies [4, 5, 20]. The progressive decline in metabolic activity from NC to aMCI then AD is consistent with the severity of cognitive impairment. The ICC seed regions closely overlapped with the PCC/RSC region affected by AD based on our PET analyses, confirming our choice of using ICCs as the key seed regions for detailed functional and structural connectivity analyses of the DMN. Our whole-brain ICC seed-based connectivity analyses demonstrated the general trend of progressively declining functional and structural connections between the ICCs and the rest of the DMN due to AD, although this effect varied by region and was more right-lateralized in our subject cohort. This variability was probably due to a relatively small sample size and an inherently heterogeneous subject population. However, the consistent finding of both weakened functional and structural connections between right ICC and MePFC demonstrates that this AD-related alteration in the DMN is significant. Our findings on functional connectivity are consistent with the recent study by Binnewijzend et al. [7]. With a much larger sample size (39 AD, 23 MCI, and 43 NC), they applied independent component analyses and found that AD reduced functional connectivity within the DMN in the precuneus and PCC, comparing to NC, and

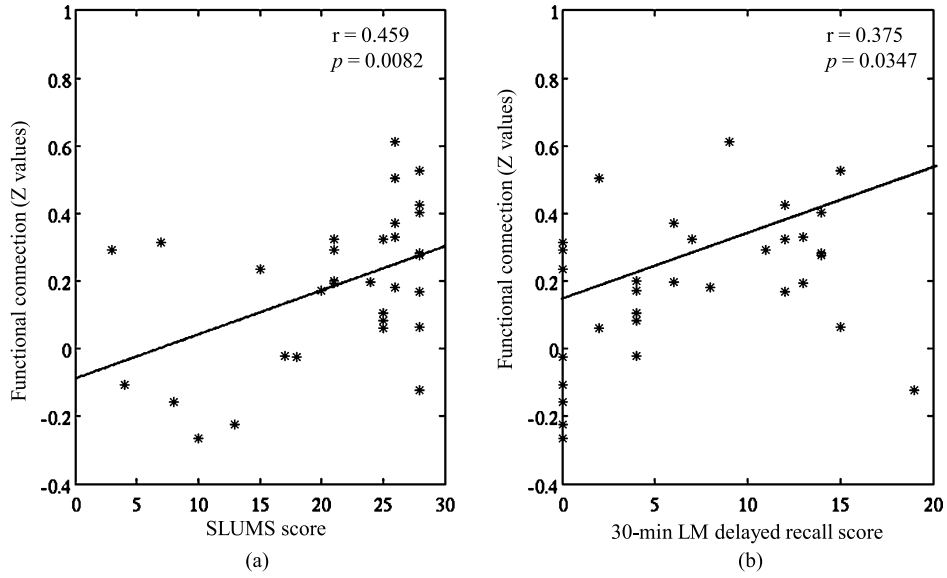

Fig. 9. With all subjects included, the significant correlations were shown between the left isthmus of cingulate cortex-right hippocampus functional connection (the Fisher's Z-transformed values of the correlations) and (a) SLUMS score and (b) 30-min LM (logical memory) delayed recall score.

progressively declining functional connection from NC to MCI then AD. However, our ICC seed based technique revealed further affected regions due to AD within the DMN. These additional regions are consistent with the recent study by Zhang et al. [17], who used a seed at PCC as well. Additional regions found to have reduced functional connectivity with ICC (bilateral TPJCs, PCC/RSC, and right hippocampus) due to AD also located at regions with reduced metabolic activity, as expected. The reduced functional connectivity due to AD between left ICC and right hippocampus identified from whole-brain analyses was consistent with the significant correlations between this connectivity and metabolic activity (reflected by PET signal) at the left ICC as well as at the right hippocampus. It was also consistent with the significant correlations between this connectivity and cognitive scores (SLUMS or LM-dr). The PET-functional connectivity correlation analyses demonstrated a direct relationship between regional neuronal metabolic decline and degree of functional disconnection among nodes of the DMN. These findings are corroborated by those from the atrophy-functional connectivity correlation analyses, where the left ICC cortical thickness was found to be significantly correlated with the functional connectivity between ICC and bilateral hippocampi. We observed a significant decline in both metabolic activity and cortical thickness of the left ICC due to AD, and found these changes to be inter-related among all our subjects.

These results from multiple aspects of our integration analyses strongly support the interpretation that neuronal damage or cell death in the left ICC may lead to the weakened functional connection between the left ICC and the rest of the DMN. The reduction of metabolic activity (NC > AD and NC > aMCI) in right ICC and right and left TPJCs (NC > AD), as well as the significant correlations between metabolic activity and cortical thickness in right ICC, may help explain the weakened structural connection along the cingulum to MePFC and the weakened functional connection to right and left TPJCs. As discussed in Buckner's review paper [22], the PCC serves as a hub for information integration from the MTL (including the hippocampus) and MePFC (including MeFC, ACC, and some regions in the SFC). The weakened connectivity and communication of ICCs with hippocampi and MePFC, as found in this study, could explain a decline of cognitive function in general and episodic memory specifically. This interpretation is supported by the significant correlations between the left ICC-right hippocampus functional connectivity and cognitive scores (SLUMS or LM-dr) that we found in our subjects.

Some results are difficult to explain, particularly our anatomically asymmetric findings regarding connectivity. Compared to AD, NC subjects had significantly

stronger functional connection to TPJC and stronger structural connection to MePFC from right ICC, but not left ICC. Conversely, NC showed significantly stronger functional connections than AD between left ICC and right hippocampus, but not between right ICC and left hippocampus. Our relatively small sample size and high between-subject variation could lead to the asymmetric findings. However, asymmetric findings are not unusual. In the recent study published by Zhang et al. [17], when they compared the functional connectivity to PCC between NC and severe AD, they found significant difference at the right, but not the left, inferior parietal cortex. Interestingly, a recent paper by Royall et al. also demonstrated a right hemisphere bias in the components of the DMN based on the association between gray matter atrophy and dementia severity in their study of early AD and older adults without dementia [39].

We did not find many differences between our AD and aMCI groups on both functional and structural connectivity in the DMN either. This could be again related to our relatively small sample size, as well as the fact that most of our AD patients were at a milder stage of their disease. Supporting the latter assertion, in particular, is the finding that our aMCI and AD groups exhibited similar degrees of episodic memory dysfunction. Alternatively, the lack of differences between AD and aMCI groups may be related to the heterogeneity of MCI as a clinical entity. This heterogeneity is also reflected by the study by Binnewijzend et al. [7], who only found significant functional connectivity difference between AD and stable MCI patients. While many MCI patients progress to AD-type dementia, others may develop non-AD dementia (e.g., vascular dementia), stay cognitively stable, or even revert to normal cognitive status [2, 40]. In a meta-analysis of inception cohort studies, Mitchell and Shiri-Feshki [40] estimated that in specialist settings, only about 39% of MCI patients defined using the Mayo Clinic/Petersen criteria for amnestic MCI [27] developed dementia over a follow-up of 3–10 years.

The purpose of integrating functional and structural connectivity analyses in this study was to better understand AD-related alterations in the DMN. We demonstrated a unique approach by specifically defining subject-specific ICC seeds for functional connectivity analysis and their associated WM regions as seeds for structural connectivity analysis. This approach should provide a high level of specificity. We applied a probabilistic tracking technique, which should be more robust with respect to the uncertainty in fiber orientation at regions with low diffusion anisotropy (especially near gray matter) [41] and thus was preferred over a deterministic approach [42], which is generally limited to high diffusion anisotropy regions. We expected to find WM tracts connecting each of the functionally connected gray matter regions of the DMN. With our method, significant structural and functional connections between ICC and MePFC were seen in our NC group, as expected; significant structural connectivity differences between AD and NC were found in the cingulum, a WM tract that directly connects ICCs and MePFC. Some significant clusters were also noted in other DMN pathways, but these pathways contain low-density and crossing fibers and potentially indirect structural fiber connections, and thus it is difficult to assess their structural connectivity alternation due to AD with DWI-based fiber tracking [18, 38].

The DMN was originally defined based on patterns of brain function. We have limited our anatomical ROI-based analyses to bilateral ICCs and hippocampi because they can be well defined with a high level of specificity in each subject. These regions also correspond well to the key components of the DMN (PCC/RSC and MTL). MePFC and TPJC (the other components of the DMN) are large and contain multiple anatomical subregions. High levels of variation in atrophy and morphology due to AD [43] and even normal aging are expected with these regions. Thus, MePFC and TPJC cannot be used as robust, well-circumscribed seed regions in connectivity analyses. The correlation with metabolic activity at these two DMN components was only demonstrated through qualitative comparison on whole-brain analyses of rs-fMRI and PET.

CONCLUSIONS

Our whole-brain group and region of interest-based analyses demonstrated that AD weakens the structural and functional connections between ICC and other regions within the DMN, consistent with regional reduction of metabolic activity and atrophy within the DMN. A progressive weakening trend of these connections was also observed from NC to aMCI and then AD, although significant differences between aMCI and the other two groups were not found. Overall, based on both FDG-PET and MRI results, the DMN appears to serve as a window to understanding structural and functional brain changes associated with AD and aMCI.

ACKNOWLEDGMENTS

The authors thank Scarlett Doyle for scanning support and research assistants Holly Nieusma, Sarah Kiel, and Colleen Osak for subject recruitment. This work was partially supported by the Intramural Research Grants Program, as well as the Departments of Radiology and Psychology at Michigan State University.

Authors' disclosures available online (http://www.j-alz.com/disclosures/view.php?id=1617).

REFERENCES

[1] Querfurth HW, LaFerla FM (2010) Alzheimer's disease. *N Engl J Med* **362**, 329-344.

[2] Petersen RC, Roberts RO, Knopman DS, Boeve BF, Geda YE, Ivnik RJ, Smith GE, Jack CR Jr (2009) Mild cognitive impairment: Ten years later. *Arch Neurol* **66**, 1447-1455.

[3] Jack CR Jr, Petersen RC, Xu YC, Waring SC, O'Brien PC, Tangalos EG, Smith GE, Ivnik RJ, Kokmen E (1997) Medial temporal atrophy on MRI in normal aging and very mild Alzheimer's disease. *Neurology* **49**, 786-794.

[4] Mosconi L, Tsui WH, Herholz K, Pupi A, Drzezga A, Lucignani G, Reiman EM, Holthoff V, Kalbe E, Sorbi S, Diehl-Schmid J, Perneczky R, Clerici F, Caselli R, Beuthien-Baumann B, Kurz A, Minoshima S, de Leon MJ (2008) Multicenter standardized 18F-FDG PET diagnosis of mild cognitive impairment, Alzheimer's disease, and other dementias. *J Nucl Med* **49**, 390-398.

[5] Minoshima S, Giordani B, Berent S, Frey KA, Foster NL, Kuhl DE (1997) Metabolic reduction in the posterior cingulate cortex in very early Alzheimer's disease. *Ann Neurol* **42**, 85-94.

[6] Bai F, Shi Y, Yuan Y, Wang Y, Yue C, Teng Y, Wu D, Zhang Z, Jia J (2012) Altered self-referential network in resting-state amnestic type mild cognitive impairment. *Cortex* **48**, 604-613.

[7] Binnewijzend MA, Schoonheim MM, Sanz-Arigita E, Wink AM, van der Flier WM, Tolboom N, Adriaanse SM, Damoiseaux JS, Scheltens P, van Berckel BN, Barkhof F (2012) Resting-state fMRI changes in Alzheimer's disease and mild cognitive impairment. *Neurobiol Aging* **33**, 2018-2028.

[8] Chen G, Ward BD, Xie C, Li W, Wu Z, Jones JL, Franczak M, Antuono P, Li SJ (2011) Classification of Alzheimer disease, mild cognitive impairment, and normal cognitive status with large-scale network analysis based on resting-state functional MR imaging. *Radiology* **259**, 213-221.

[9] Uddin LQ, Kelly AM, Biswal BB, Xavier Castellanos F, Milham MP (2009) Functional connectivity of default mode network components: Correlation, anticorrelation, and causality. *Hum Brain Mapp* **30**, 625-637.

[10] Bozoki AC, Korolev IO, Davis NC, Hoisington LA, Berger KL (2012) Disruption of limbic white matter pathways in mild cognitive impairment and Alzheimer's disease: A DTI/FDG-PET Study. *Hum Brain Mapp* **33**, 1792-1802.

[11] Wang L, Goldstein FC, Levey AI, Lah JJ, Meltzer CC, Holder CA, Mao H (2011) White matter hyperintensities and changes in white matter integrity in patients with Alzheimer's disease. *Neuroradiology* **53**, 373-381.

[12] Raichle ME, MacLeod AM, Snyder AZ, Powers WJ, Gusnard DA, Shulman GL (2001) A default mode of brain function. *Proc Natl Acad Sci U S A* **98**, 676-682.

[13] Bai F, Zhang Z, Yu H, Shi Y, Yuan Y, Zhu W, Zhang X, Qian Y (2008) Default-mode network activity distinguishes amnestic type mild cognitive impairment from healthy aging: A combined structural and resting-state functional MRI study. *Neurosci Lett* **438**, 111-115.

[14] Greicius MD, Srivastava G, Reiss AL, Menon V (2004) Default-mode network activity distinguishes Alzheimer's disease from healthy aging: evidence from functional MRI. *Proc Natl Acad Sci U S A* **101**, 4637-4642.

[15] Greicius MD, Supekar K, Menon V, Dougherty RF (2009) Resting-state functional connectivity reflects structural connectivity in the default mode network. *Cereb Cortex* **19**, 72-78.

[16] Supekar K, Menon V, Rubin D, Musen M, Greicius MD (2008) Network analysis of intrinsic functional brain connectivity in Alzheimer's disease. *PLoS Comput Biol* **4**, e1000100.

[17] Zhang HY, Wang SJ, Liu B, Ma ZL, Yang M, Zhang ZJ, Teng GJ (2010) Resting brain connectivity: Changes during the progress of Alzheimer disease. *Radiology* **256**, 598-606.

[18] Woolsey TA, Hanaway J, Gado MH (2003) *The brain atlas: A visual guide to the human central nervous system*, John Wiley & Sons, Inc., Hoboken, New Jersey.

[19] Andrews-Hanna JR, Snyder AZ, Vincent JL, Lustig C, Head D, Raichle ME, Buckner RL (2007) Disruption of large-scale brain systems in advanced aging. *Neuron* **56**, 924-935.

[20] Matsuda H (2001) Cerebral blood flow and metabolic abnormalities in Alzheimer's disease. *Ann Nucl Med* **15**, 85-92.

[21] Small GW, Ercoli LM, Silverman DH, Huang SC, Komo S, Bookheimer SY, Lavretsky H, Miller K, Siddarth P, Rasgon NL, Mazziotta JC, Saxena S, Wu HM, Mega MS, Cummings JL, Saunders AM, Pericak-Vance MA, Roses AD, Barrio JR, Phelps ME (2000) Cerebral metabolic and cognitive decline in persons at genetic risk for Alzheimer's disease. *Proc Natl Acad Sci U S A* **97**, 6037-6042.

[22] Buckner RL, Andrews-Hanna JR, Schacter DL (2008) The brain's default network: Anatomy, function, and relevance to disease. *Ann N Y Acad Sci* **1124**, 1-38.

[23] Tariq SH, Tumosa N, Chibnall JT, Perry MH, 3rd, Morley JE (2006) Comparison of the Saint Louis University mental status examination and the mini-mental state examination for detecting dementia and mild neurocognitive disorder–a pilot study. *Am J Geriatr Psychiatry* **14**, 900-910.

[24] Sheikh J, Yesavage J (1986) Geriatric Depression Scale (GDS): Recent evidence and development of a shorter version. *In Clinical Gerontology: A Guide to Assessment and Intervention*. The Haworth Press, New York, pp. 165-173.

[25] Folstein MF, Folstein SE, McHugh PR (1975) Mini-mental state. A practical method for grading the cognitive state of patients for the clinician. *J Psychiatr Res* **12**, 189-198.

[26] McKhann G, Drachman D, Folstein M, Katzman R, Price D, Stadlan EM (1984) Clinical diagnosis of Alzheimer's disease: Report of the NINCDS-ADRDA Work Group under the auspices of Department of Health and Human Services Task Force on Alzheimer's Disease. *Neurology* **34**, 939-944.

[27] Petersen RC, Smith GE, Waring SC, Ivnik RJ, Tangalos EG, Kokmen E (1999) Mild cognitive impairment: Clinical characterization and outcome. *Arch Neurol* **56**, 303-308.

[28] Fischl B, Salat DH, Busa E, Albert M, Dieterich M, Haselgrove C, van der Kouwe A, Killiany R, Kennedy D, Klaveness S, Montillo A, Makris N, Rosen B, Dale AM (2002) Whole brain segmentation: Automated labeling of neuroanatomical structures in the human brain. *Neuron* **33**, 341-355.

[29] Kiebel SJ, Ashburner J, Poline JB, Friston KJ (1997) MRI and PET coregistration–a cross validation of statistical parametric mapping and automated image registration. *Neuroimage* **5**, 271-279.

[30] Smith SM, Jenkinson M, Woolrich MW, Beckmann CF, Behrens TE, Johansen-Berg H, Bannister PR, De Luca M, Drobnjak I, Flitney DE, Niazy RK, Saunders J, Vickers J, Zhang Y, De Stefano N, Brady JM, Matthews PM (2004) Advances in functional and structural MR image analysis and implementation as FSL. *Neuroimage* **23** (Suppl 1), S208-S219.

[31] Cox RW (1996) AFNI: Software for analysis and visualization of functional magnetic resonance neuroimages. *Comput Biomed Res* **29**, 162-173.

[32] Ward B (2000) *Deconvolution analysis of fMRI time series Data*, Milwaukee.

[33] Fox MD, Snyder AZ, Vincent JL, Corbetta M, Van Essen DC, Raichle ME (2005) The human brain is intrinsically organized into dynamic, anticorrelated functional networks. *Proc Natl Acad Sci U S A* **102**, 9673-9678.

[34] Behrens TE, Berg HJ, Jbabdi S, Rushworth MF, Woolrich MW (2007) Probabilistic diffusion tractography with multiple fibre orientations: What can we gain? *Neuroimage* **34**, 144-155.

[35] Behrens TE, Woolrich MW, Jenkinson M, Johansen-Berg H, Nunes RG, Clare S, Matthews PM, Brady JM, Smith SM (2003) Characterization and propagation of uncertainty in diffusion-weighted MR imaging. *Magn Reson Med* **50**, 1077-1088.

[36] Ward B (2000) *Simultaneous inference for fMRI data*, Milwaukee.

[37] Kinahan P, Vesselle H, Williams J, Stearns C, Schmitz R, Alessio A, Macdonald L, Mawlawi O, Turkington T, Lewellen T (2006) Performance evaluation of an integrated PET/CT scanner: Discovery STE. *J Nucl Med* **47**, 392P.

[38] Zhu DC, Majumdar S (2012) Integration of resting-state fMRI and diffusion-weighted MRI connectivity analyses of the human brain: Limitations and improvement. *J Neuroimaging* doi: 10.1111/j.1552-6569.2012.00768.x

[39] Royall DR, Palmer RF, Vidoni ED, Honea RA, Burns JM (2012) The default mode network and related right hemisphere structures may be the key substrates of dementia. *J Alzheimers Dis* **32**, 467-478.

[40] Mitchell AJ, Shiri-Feshki M (2009) Rate of progression of mild cognitive impairment to dementia–meta-analysis of 41 robust inception cohort studies. *Acta Psychiatr Scand* **119**, 252-265.

[41] Behrens TE, Johansen-Berg H, Woolrich MW, Smith SM, Wheeler-Kingshott CA, Boulby PA, Barker GJ, Sillery EL, Sheehan K, Ciccarelli O, Thompson AJ, Brady JM, Matthews PM (2003) Non-invasive mapping of connections between human thalamus and cortex using diffusion imaging. *Nat Neurosci* **6**, 750-757.

[42] Mori S, Crain BJ, Chacko VP, van Zijl PC (1999) Three-dimensional tracking of axonal projections in the brain by magnetic resonance imaging. *Ann Neurol* **45**, 265-269.

[43] Karas GB, Scheltens P, Rombouts SA, Visser PJ, van Schijndel RA, Fox NC, Barkhof F (2004) Global and local gray matter loss in mild cognitive impairment and Alzheimer's disease. *Neuroimage* **23**, 708-716.